Electronic Couplings for Resonance Energy Transfer from CCSD Calculations: From Isolated to Solvated Systems

Marco Caricato,*,[†] Carles Curutchet,[‡] Benedetta Mennucci,[¶] and Giovanni Scalmani[§]

[†]Department of Chemistry, University of Kansas, 1251 Wescoe Hall Drive, Lawrence, Kansas 66045, United States

[‡]Departament de Fisicoquímica, Facultat de Farmàcia, Universitat de Barcelona, Av. Joan XXIII s/n, 08028 Barcelona, Spain

[¶]Dipartimento di Chimica e Chimica Industriale, University of Pisa, via G. Moruzzi 3, 56124 Pisa, Italy

[§]Gaussian, Inc., 340 Quinnipiac Street, Building 40, Wallingford, Connecticut 06492, United States

Ⓢ Supporting Information

ABSTRACT: Quantum mechanical (QM) calculations of electronic couplings provide great insights for the study of resonance energy transfer (RET). However, most of these calculations rely on approximate QM methods due to the computational limitations imposed by the size of typical donor–acceptor systems. In this work, we present a novel implementation that allows computing electronic couplings at the coupled cluster singles and doubles (CCSD) level of theory. Solvent effects are also taken into account through the polarizable continuum model (PCM). As a test case, we use a dimer of indole, a common model system for tryptophan, which is routinely used as an intrinsic fluorophore in Förster resonance energy transfer studies. We consider two bright $\pi \rightarrow \pi^*$ states, one of which has charge transfer character. Lastly, the results are compared with those obtained by applying TD-DFT in combination with one of the most popular density functionals, B3LYP.
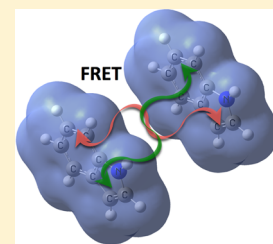
1. INTRODUCTION

Resonance energy transfer (RET) is of fundamental importance in many natural processes, of which the most notable is photosynthesis.[1] RET occurs when an excited donor (D) system transfers energy nonradiatively to an acceptor (A) system, which does not need to be bonded or even in close proximity to the donor. In fact, efficient energy transfer can occur even if the donor–acceptor pair is separated by tens of Å. RET has also become an important process for a variety of applications. It can be used to probe distances between large biomolecules (i.e., as a spectroscopic ruler), even at the single-molecule level, or as a means to transfer energy between man-made compounds, thus entering the realm of materials and energy science.[2–6]

A large part of our ability to predict and interpret RET processes is due to the theory developed by Förster in the late 1940s.[7,8] There are two key aspects of Förster theory. The first is the assumption of a weak-coupling transfer regime, thus adopting a golden rule expression for the rate. The second is the approximation of the electronic coupling as a dipole–dipole interaction between the transition electric dipole moments characterizing donor and acceptor excitations. As a result, the RET rate, which depends quadratically on the energy coupling, will present a negative-sixth power dependence on the D–A distance. This formula assumes that the interaction between chromophores is weak such that the coupling can be computed through perturbation theory. Thus, the transition dipoles for the chromophores can be computed independently and subsequently used to evaluate their mutual interaction. In experimental practice, the power of the Förster theory arises

from the fact that such dipoles, and therefore the RET rate, can be estimated from purely spectroscopic observables.

An improvement over the simple dipole–dipole interaction can be achieved with modern quantum chemistry methods, where the coupling is expressed as the Coulomb interaction between the three-dimensional transition densities.[9–19] These densities can also be used to introduce other quantum mechanical effects, such as exchange and correlation, and to account for electron density overlap. This improvement over Förster theory is still based on perturbation theory, i.e., the transition densities of the two systems are computed separately, and the interaction is turned on in a later step without considering any relaxation processes. This approximation, however, has been shown to accurately reproduce the "exact" coupling obtained from supermolecule calculations at distances as close as 5 Å.[11]

Another important issue to consider in the modeling of RET is the effect of the environment, particularly a solvent. This effect can be divided in an implicit and an explicit term.[20] The implicit contribution is related to the polarization of the electronic densities of the involved chromophores, whereas the explicit term is due to the effect that the polarization of the environment has on their interaction.[9,11,12,21] Both terms can still be treated perturbatively such that the solvated species can be treated independently.

From this brief introduction, it should appear evident that an accurate modeling of the RET rate, even remaining in the limit of weak-coupling, is a difficult task. Quantum mechanical

methods coupled to solvation models surely represent a valid strategy, although, a delicate issue arises from the fact that most chromophores of interest in RET studies, either in the field of biology and biochemistry, or in the field of materials and energy science, are large molecular or even supramolecular systems. The intrinsic complexity of the electronic structure of these compounds, when coupled with the environment effects and with the necessity to consider averages over all possible conformations of the chromophores in order to simulate experimental results, poses a limit to the computational methods that can be reasonably afforded. The largest majority of RET calculations is thus based on approximated density functional theory (DFT) methods, and semiempirical methods as Zerner's intermediate neglect of differential overlap (ZINDO)[22] may become unavoidable for even larger systems. The limitations of such methods are well-known, e.g., impossible to systematically improve a given approximate method, and system-dependent quality of the results.

The scope of this work is to go beyond these approximate methods and compute the electronic coupling with a high level wave function method: coupled cluster with single and double excitations (CCSD).[23] We present the first calculations of electronic coupling in gas phase and in solution at this level of theory. Transition properties are evaluated with linear response theory,[24−26] and the solvent effect is introduced with the polarizable continuum model (PCM).[27−34] The results obtained with this methodology may be used for calibration of less accurate but more computationally efficient methods. In this work, we compare CCSD results with those obtained with the most popular DFT method, B3LYP.[35−37]

As a test case, we consider the dimer of indole, a model molecule that represents the main chromophoric moiety of tryptophan, the amino acid mainly responsible for the intrinsic fluorescent properties of proteins. Tryptophan is a popular fluorescence probe in fluorescence resonance energy transfer (FRET) studies because its use does not involve any altering of the protein structure as instead it is the case when an external organic fluorophore is considered.[38,39] Moreover, the intrinsic fluorescence of proteins, a property exploited in a plethora of techniques in biochemistry, often involves energy transfers among tryptophans prior to emission.[40] Understanding RET among indole moieties, thus, is of importance to develop microscopic models able to predict the often complex outcome of such experiments. In particular, we consider various separation distances and various relative orientations between the monomers to obtain a reasonable spatial averaging.

The paper is organized as follows. Section 2 discusses the theory for the energy coupling calculations, and section 3 presents the details of how we performed these calculations. The numerical results are presented in section 4. A general discussion of our findings and concluding remarks are reported in section 5.

2. METHODS

The rate of electronic energy transfer in the weak coupling regime can be computed by the Fermi golden rule expression[7,8]

$$k = \frac{2\pi}{\hbar}|V|^2 J \tag{1}$$

where V is the electronic coupling between the donor and acceptor chromophores, and J is the normalized spectral overlap between donor emission and acceptor absorption spectra. As commented in the Introduction, Förster approxi-

mated the electronic coupling as only due to the Coulomb interaction between the transition dipole moments of the states involved in the energy transfer

$$V^{Cou} = \frac{\kappa \mu_D \mu_A}{n^2 r^3} \tag{2}$$

where the subscripts D and A refer to the donor and acceptor chromophores, respectively, separated by the distance r. κ is the orientation factor, a geometrical parameter that takes into account the relative orientation of the dipole moments μ_D and μ_A. The formula in eq 2 also takes into account the screening effect of the solvent through the $1/n^2$ factor, where n is the refractive index of the solvent.

The formula in eq 2 considerably simplifies the calculation of the coupling because the donor and acceptor species can be considered as separated entities, and the coupling is computed from the unperturbed transition dipoles estimated from optical spectra of the respective solvated dyes.[41] However, eq 2 neglects important contributions: a proper three-dimensional account of the electron density, other quantum-mechanical interactions like electronic exchange and correlation, and a realistic description of the solvent effect. The first two issues can be taken into account by using quantum chemistry methods, and the latter issue can be recovered by employing a proper solvation model. In the present study, a continuum description has been adopted by using the PCM approach. Within this formalism, the response of the solvent is described in terms of an apparent surface charge on the cavity that embeds the interacting species. By combining a full quantum mechanical (QM) description of the D and A species with the PCM description of the solvent, the coupling can be rewritten as[11,12]

$$\begin{aligned} V &= V^{Cou} + V^{PCM} \\ &= \int d\mathbf{r}\, d\mathbf{r}'\rho_D^\dagger(\mathbf{r}')\frac{1}{|\mathbf{r}-\mathbf{r}'|}\rho_A(\mathbf{r}) \\ &\quad + \sum_k \left(\int d\mathbf{r}\rho_D^\dagger(\mathbf{r})\frac{1}{|\mathbf{r}-\mathbf{s}_k|}\right)q(s_k;\, \varepsilon_\omega, \rho_A) \end{aligned} \tag{3}$$

where ρ_D (ρ_A) is the transition density for the donor (acceptor). The first term on the right-hand side of eq 3 represents the generalization of the "dipole−dipole" interaction, and it accounts for the full Coulomb interaction between the D and A transition densities. The second term is the explicit solvent term, where the interaction is given by the electrostatic potential generated by the donor transition density on the cavity surface (in parentheses) and the PCM apparent surface charges located on the discretized surface (s_k positions). The PCM charges depend on the acceptor transition density and on the frequency dependent dielectric constant of the medium, which in practical calculations is approximated by the optical dielectric constant ε_∞, i.e., the square of the index of refraction of the solvent. Depending on which QM method is used, further terms can be added to account for exchange and correlation effects as well as for the overlap between the two transition densities. For allowed transitions as the ones studied here, these additional terms are negligible, and the coupling is fully determined by Coulomb plus solvent effects only. The solvent effect is introduced through PCM within the linear response nonequilibrium regime, where the slow component of the solvent polarization (i.e., the nuclear and collective molecular motion of the solvent molecules) is frozen in

equilibrium with the ground state. This approximation assumes that the RET occurs at a rate faster than geometrical relaxations for both the solute and solvent, and it is consistent with the screening factor introduced by Förster (see eq 2). We refer the reader to refs 11 and 12 for more details on the evaluation of eq 3.

Any QM method can in principle be used to compute the transition densities in eq 3. In practice, however, the size of the systems that are relevant to experimentalists poses a limit to the quality of the methods that can be used in the simulations. Most calculations resort to time dependent density functional theory (TD-DFT) or to semiempirical methods, such as Zerner's intermediate neglect of differential overlap (ZINDO).[22] Highly accurate methods like those belonging to coupled cluster theory (CC)[23] are often outside the applicability range. Fückel and co-workers presented previous calculations at the second-order approximate coupled-cluster (CC2) level of theory, although limited to gas phase.[42] In this study, we present the first application of a CC method with single and double excitations (CCSD) to study electronic coupling in gas phase and in solution. For a CC method to be used, a slight modification to eq 3 must be introduced due to the non-Hermitian nature of the CC similarity transformed Hamiltonian

$$\bar{H} = e^{-\hat{T}} \hat{H} e^{\hat{T}} \tag{4}$$

where $\hat{T}$ is the CC excitation operator. The non-Hermiticity of $\bar{H}$ in eq 4 implies that different left-hand and right-hand transition matrices are computed for each chromophore. Therefore, each integral in eq 3 is computed as

$$V_O^{CC} = \frac{1}{2} \int d\mathbf{r} \, d\mathbf{r}' \left[\rho_D^{L\dagger}(\mathbf{r}') \hat{O} \rho_A^R(\mathbf{r}) + \left(\rho_A^{L\dagger}(\mathbf{r}') \hat{O}^{\dagger} \rho_D^R(\mathbf{r}) \right)^* \right] \tag{5}$$

where the superscripts L and R refer to the left- and right-hand transition densities,[43] respectively, and $\hat{O}$ is any of the operators in eq 3. For the definition of the transition density, we use the equation of motion approach of Stanton and Bartlett[26] rather than the size intensive linear response definition[44] because the former has been shown to be numerically equivalent to the latter for systems of size comparable to those treated here, both in gas phase and in solution,[34,45] and it is computationally cheaper.

A quantity that is of great interest for understanding the importance of solvation effects on the electronic coupling, and thus on the rate of the energy transfer, is solvent screening. This can be defined as[21]

$$s = \frac{V^{Cou} + V^{PCM}}{V^{Cou}} \tag{6}$$

where V^{Cou} and V^{PCM} are the Coulomb and the explicit solvent contribution to the coupling (first and last terms in eq 3); V^{Cou} is also computed in solution. Hence, s in eq 6 allows for distinguishing the direct electrostatic contribution of the solvent to the electronic coupling from its indirect contribution deriving from the polarization of the electronic density of the chromophores.

3. COMPUTATIONAL DETAILS

All calculations are performed on a dimer of indole, shown in two representative orientations in Figure 1. Multiple geometries
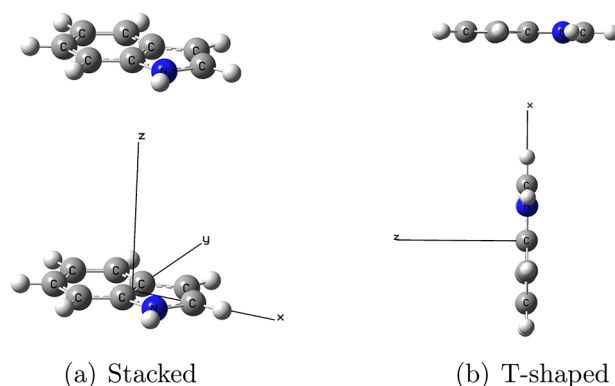

(a) Stacked   (b) T-shaped

Figure 1. Structures of the stacked and T-shaped configurations of the indole dimer.

of the dimer are considered, which we will call "configurations" in the following. The dimer configurations are built starting from two identical monomers completely overlapped and with their center of mass (COM) in the origin of the reference system. From this initial position, one of the monomers is maintained as fixed while the other is moved. Let us call the fixed monomer **1** and the moving monomer **2**. First, monomer **2** is rigidly rotated around each axis. We chose four angles for the rotation: 0, $\pi/2$, π, and $3\pi/2$. Obviously, angle 0 will correspond to a pure translation. After rotation, monomer **2** is translated along one of the Cartesian axes in the positive direction. We chose four distances for the translation of the COM of **2**: 6, 8, 10, and 12 Å. The rotation plus translation is performed for each Cartesian axis. Therefore, we consider 3*3*3 + 3 = 30 different orientations for each translation distance. However, for the shortest distance, 6 Å, several configurations put the two molecules too close to each other and must be discarded. Thus, only 27 configurations are left at 6 Å. The geometries of the dimer at 8 Å distance are reported in the Supporting Information. We did not perform calculations at CCSD level for the 12 Å distance to reduce the computational burden. In fact, at this distance, the coupling for such small molecules is going to be very small and the comparison between methods not very informative.

The calculations are performed with the B3LYP hybrid functional and the CCSD method with the aug-cc-pVDZ basis set.[46,47] We use the symmetric version[48] of the integral equation formalism (IEF) version of PCM for the calculations in water solution. The cavity is built by using the radii defined for the solvation model with density (SMD),[49] and spheres are added to fill out regions around the molecules not accessible to the solvent.[50] In the dimer calculations, the entire dimer cavity is used during the monomer subcalculations. We also employ the continuous surface charge model for PCM[51] in the nonequilibrium regime ($\varepsilon = 78.36$ and $\varepsilon_\infty = n^2 = 1.78$). The geometry of the indole monomer is obtained at the B3LYP/aug-cc-pVDZ level in gas and in solution. This geometry is then used in each dimer calculation where translations and rotations are performed rigidly, as mentioned above. All calculations are performed with a development version of the Gaussian suite of programs.[52]

4. RESULTS

In this section, we report the results obtained for the indole dimer in the different configurations described in section 3. For each configuration, two $\pi \rightarrow \pi^*$ states are considered: L_a and L_b, which are involved in the intrinsic fluorescence of proteins, as well as in FRET studies involving tryptophan.[38−40] The calculated and available experimental data for the two states of the monomer in gas phase and in solution are reported in Table 1. Table 2 reports energy and property differences between the

Table 1. Experimental[53−56] and Theoretical Excitation Energies (ω in eV), Dipole Strengths (D in a.u.), and Oscillator Strengths (f) for L_a and L_b Transitions of the Indole Monomer in Gas Phase and in Solution

		gas			water		
		exp.	B3LYP	CCSD	exp.	B3LYP	CCSD
L_b	ω	4.37	4.86	4.87		4.85	4.87
	D	0.19	0.29	0.24		0.39	0.32
	f	0.02	0.04	0.03		0.05	0.04
L_a	ω	4.88	4.70	5.27	4.59	4.62	5.15
	D	1.09	0.63	0.79		0.89	1.07
	f	0.13	0.07	0.10		0.10	0.14

Table 2. Experimental and Theoretical Shifts of the Monomer Transition Properties

		$\Delta_{a-b}^{\mathrm{Gas}}$ [a]			$\Delta_a^{\mathrm{Gas-Water}}$ [b]		
		exp.	B3LYP	CCSD	exp.	B3LYP	CCSD
	ω	0.51	−0.16	0.40	0.29	0.08	0.12
L_b	D	0.90	0.34	0.55		0.26	0.28
	f	0.11	0.03	0.07		0.03	0.04

[a]Gas phase difference between L_a and L_b states. [b]Solvatochromic shift for the L_a state.

L_a and L_b states in gas phase and solvatochromic shifts for the L_a state. The tables include the excitation energy "ω", the dipole strength "D", which is the length of the electric transition dipole moment squared, and the oscillator strength "f", which is proportional to the probability of absorption toward that state and is related to the excitation energy and dipole strength through the formula

$$f = \frac{2}{3}\omega D \tag{7}$$

The excitations are reported in the order they appear in the experimental spectrum:[53−57] the L_b state at lower energy and with a smaller oscillator strength, and the L_a state at higher energy with a larger oscillator strength. L_a has a partial charge transfer character from the six-member ring toward the N center. L_b does not have the same charge transfer character, but the transition dipole is still oriented from the six-member to the five-member ring. This state does have, however, a charge-transfer character (and larger oscillator strength) in tryptophan due to the polar amino-acid chain connected to the indole ring. The transition dipoles from B3LYP in gas phase are depicted in Figure 2, and they are qualitatively similar for both methods in both environments.

The data in Table 1 shows that B3LYP and CCSD are in good agreement with each other for the L_b state in gas phase, although they overestimate the experimental result by 0.5 eV. This discrepancy may be due to limitations in the basis set, level
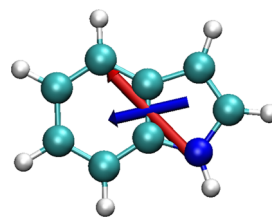

Figure 2. Transition dipoles for the L_a (red) and L_b (blue) states.

of electron correlation, lack of vibronic corrections, and possible experimental errors. Recent results using the algebraic diagrammatic construction (ADC) scheme of the polarization propagator method[56] on indole showed that passing from second to third order the excitation energy for the L_b state decreases by ∼0.2 eV, thus toward the experimental data. The effect of the solvent is minimal on this transition. For the L_a state, conversely, B3LYP largely underestimates the excitation energy, predicting this state to be below the L_b state. CCSD predicts the correct order of the states. The fact that B3LYP provides a value of excitation energy closer to experiment than CCSD (see Table 1) is fortuitous because the data in Table 2 shows the wrong trend for B3LYP. As for the oscillator strength, the agreement of CCSD with experiment is considerably better than B3LYP both in terms of absolute values and trends. Experimental data in water is only available for the L_a transition energy. The data in Table 1 shows a better agreement of B3LYP with experiment than CCSD. However, the solvatochromic shift in Table 2 shows that CCSD recovers more of the polarization due to the solvent than B3LYP. In both cases, the shift is considerably smaller than the experimental one, but the trend is correct. This is likely due to the difficulties of continuum solvation models in describing explicit solute−solvent interactions accurately. Nonetheless, PCM provides the correct trend at a moderate computational cost. Additionally, PCM provided screening effects in calculations of energy transfer coupling that are similar to those obtained with explicit polarizable solvation models[58] and subsystem TD-DFT methods.[59]

4.1. Electronic Coupling. As shown in eq 1, the RET rate is fully determined by the J parameter, which depends on the spectral properties of the two interacting species and the square of the coupling, which instead is a measure of their interaction. Here, we present an analysis of the latter term and its dependence on the geometry of the dimer as well on the solvent effect, as provided by B3LYP and CCSD.

Figure 3 reports the change of V^2 as a function of distance between the indole molecules averaged over all the configurations considered. We computed the four possible couplings between the L_a and L_b transitions with B3LYP and CCSD in gas phase and in solution. The trend across transitions is similar between levels of theory: the $L_a−L_a$ coupling is the strongest as one would expect from the value of the dipole strength for this transition (see Table 1). The $L_b−L_b$ coupling is weaker, also in agreement with the dipole strength data in Table 1. The cross couplings $L_a−L_b$ and $L_b−L_a$ are not the same because we chose translations of the centers of mass of the dimer only in the first octant of the Cartesian space. Their values are between the $L_a−L_a$ and $L_b−L_b$ for CCSD but not for B3LYP. For the latter, the $L_a−L_b$ coupling is smaller than the $L_b−L_b$ coupling, indicating that the orientation of the transition densities is less favorable for the interaction at this level of theory. The solvent effect is small for a balancing
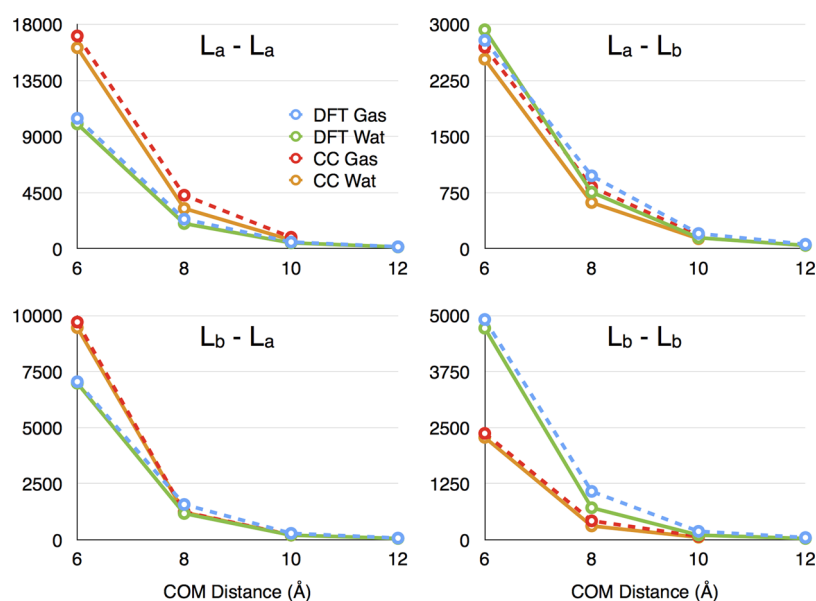
Figure 3. V^2 in $(cm^{-1})^2$ for the indole dimer at various COM distances (Å) averaged over the various orientations.
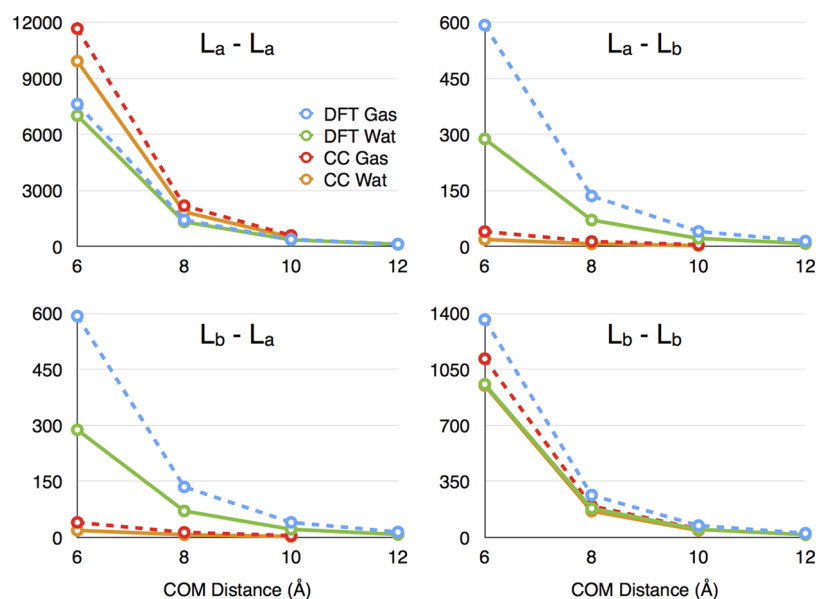

Figure 4. V^2 in $(cm^{-1})^2$ for the L_a and L_b states of the indole dimer at various COM distances (Å) for the stacked configuration.

between the solvent screening, which tends to decrease the coupling, and the larger values of the dipole strengths in solution, which tends to increase the coupling. The results in Figure 3 clearly show that B3LYP underestimates V^2_{a-a} by a factor of ~2 and overestimates V^2_{b-b} by a similar factor compared to CCSD. This is qualitatively in agreement with the trends of dipole strengths in Table 1. However, the L_b-L_b overestimation is larger than one would expect by only considering the difference in dipole strength between B3LYP and CCSD shown in Table 1. In the L_b-L_a coupling, the L_a state dominates such that CCSD provides larger values of the coupling compared to B3LYP, although the difference is considerably smaller than in the L_a-L_a case. For the L_a-L_b coupling, conversely, the L_a and L_b effects compensate, and the two methods provide very similar results with the B3LYP values slightly larger than those from CCSD.

To avoid the complications of partial conformational sampling, we also report plots of V^2 for two specific configurations: stacked and T-shaped. Pictures of these configurations are shown in Figure 1. There are multiple ways to define stacked and T-shaped configurations (rotating around the z axis for the stacked and around the x axis for the T-shaped in Figure 1), but we simply choose two as representative examples. The coupling for the stacked configuration is shown in Figure 4. The overall magnitude of the coupling for this configuration is smaller than for the average case. However, the trends between methods for V^2_{a-a} and V^2_{b-b} are similar: B3LYP underestimates CCSD for the former and overestimates it for the latter. The cross coupling is exactly the same for the L_a-L_b and L_b-L_a cases because of the symmetry of this configuration. Figure 4 shows that the cross coupling is basically negligible for CCSD, indicating that the orientation of the transition density is not favorable for energy
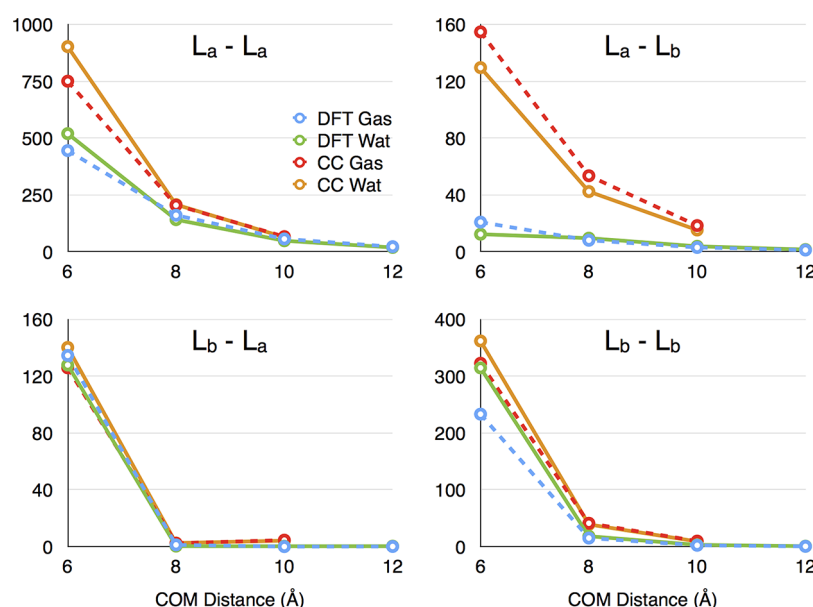
E

Figure 5. V^2 in $(cm^{-1})^2$ for the L_a and L_b states of the indole dimer at various COM distances (Å) for the T-shaped configuration.

transfer in this configuration. B3LYP shows a significant value for the cross coupling compared to CCSD but still an order of magnitude smaller than the average case. The effect of solvation is considerably larger than for the average case, which can be explained considering that in the stacked configuration there is "more solvent" between the two indoles as they face each other from the flat side. The solvent effect is larger for CCSD than for B3LYP for the L_a–L_a coupling, whereas it is the opposite for the L_b–L_b coupling, which is consistent with the values of the dipole strengths for the two transitions and the two methods shown in Table 1: a larger value of the transition dipole corresponds to a larger solvation effect in a polar solvent like water.

The results for the T-shaped configuration are reported in Figure 5. The values of the coupling are much smaller than the average values with $V^2 < 1000$ $(cm^{-1})^2$ even for the L_a–L_a combination. This result can be explained in terms of the Förster model. In fact, the transition dipoles are almost orthogonal between the monomers for both states because they reside on the molecular plane (see Figure 2). The L_a–L_b and L_b–L_a couplings are not the same for this configuration because the orientation of the transition dipoles is not equivalent. In the L_b–L_a case, the coupling goes to zero very rapidly already at 8 Å. For the L_a–L_b case, the coupling with B3LYP is rather small at every distance. Contrary to previous cases, B3LYP underestimates the coupling for all states. The solvent effect is opposite compared to the previous cases, and this is more evident at the shortest distance (6 Å). This is likely due to the shape of the PCM cavity in the region of shortest distance between the monomers. At longer distances, the solvent effect is small.

4.2. Distance Decay Rate. An interesting analysis is obtained by fitting the data of the rate as a function of distance. According to Förster theory, the decay of the transfer rate should be proportional to r^{-6}, where r is the distance between the donor and the acceptor. To check the validity of this approximation, we fit the data of the QM V^2 to a power function: Ax^{-B}, where A and B are the parameters of the fitting. The optimal data obtained from the average V^2 for the exponent B is reported in Table 3.

Table 3. Exponent B for the Power Decay Fitting of the Average V^2

	gas		water	
	B3LYP	CCSD	B3LYP	CCSD
L_a–L_a	5.3	5.0	5.6	5.7
L_a–L_b	4.2	4.4	5.0	5.1
L_b–L_a	5.4	6.3	6.3	7.2
L_b–L_b	5.5	6.1	6.7	7.0

The decay for the gas phase is slower than in Förster theory for the L_a–L_a and L_a–L_b cases, around the fifth and fourth power, respectively, for both levels of theory. The decay follows the sixth power law for the other two couplings at CCSD level, but it is still somewhat slower with B3LYP (around 5.5). In solution, the decay rate is faster across the board. It is close to the sixth power for the L_a–L_a coupling with both methods, and it is around the fifth power for the L_a–L_b coupling. The decay is faster than the sixth power for the other two couplings, and it is close to the seventh power for the L_b–L_b coupling for B3LYP and at or above the seventh power for CCSD and the L_b–L_a and L_b–L_b couplings.

The fitting data for the stacked and T-shaped configurations are reported in Table 4. Starting from the stacked configuration, the results in the table show an almost perfect sixth order decay for the L_a–L_a and L_b–L_b couplings with B3LYP and CCSD (slightly faster for the latter method). The solvent does not seem to influence the decay rate. The situation is different for the cross coupling: the decay rate is closer to the fifth power for B3LYP both in gas phase and in solution (slightly slower in the latter medium). The results for CCSD show a much slower decay, on the order of 3.8 in gas and 3.5 in solution. However, here, the fitting may be less reliable due to the overall small magnitude of the coupling as shown in Figure 4. For the T-shaped configuration, we first notice that no fitting was possible for the L_b–L_a and L_b–L_b couplings due to their small magnitude. The decay for the L_a–L_a coupling is around the fourth power for B3LYP in gas phase and 4.6 in solution. The decay is overall faster with CCSD, closer to the fifth power in gas and in solution. For the L_a–L_b coupling, the decay is on the

F

**Table 4. Exponent B for the Power Decay Fitting of V^2 for the Stacked and T-Shaped Configurations[a]**

	gas		water	
	B3LYP	CCSD	B3LYP	CCSD
Stacked				
$L_a–L_a$	5.8	5.8	5.8	5.8
$L_a–L_b$	5.2	3.8	4.9	3.5
$L_b–L_a$	5.2	3.8	4.9	3.5
$L_b–L_b$	5.7	6.0	5.8	6.1
T-shaped				
$L_a–L_a$	3.8	4.6	4.6	5.1
$L_a–L_b$	3.6	3.9	1.9	4.0
$L_b–L_a$				
$L_b–L_b$				

[a]The empty spots are for coupling values that are too small for the fitting.

order of the fourth power for all methods and media, except for B3LYP in water where the value of the fitting is clearly unreliable. The overall slower decay rates for this configuration are due to the fact that the effective distance of the transition densities is smaller than for the stacked configuration, and the approximations of the Förster regime are less applicable.

4.3. Solvent Screening. The results for the solvent screening computed as in eq 6 are compared to those obtained with the simple screening factor suggested by Förster in eq 2 $s_F = 1/n^2 = 0.56$ and with the screening factor derived from Onsager's model of solvation $s_O = 3/(2n^2 + 1) = 0.66$ (the numerical values refer to water as solvent). It is important to note that, in both of these simplified models, the solvent screening is constant independently from the distance and orientation between the donor and the acceptor as well as from the electronic transitions involved.

Figure 6 reports the solvent screening averaged over all the configurations considered. The top plot reports the B3LYP results and the bottom the CCSD results. A visual comparison between the two plots shows that the B3LYP trends are rather
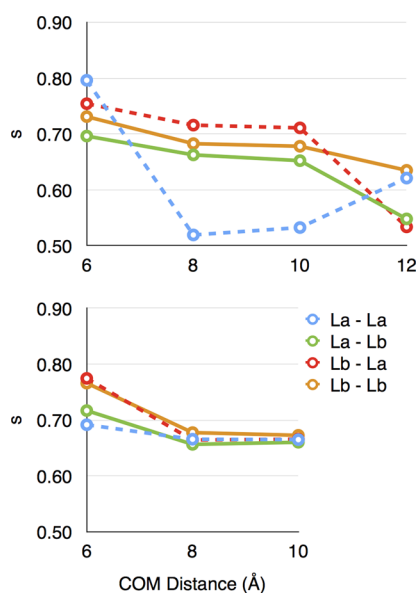
Figure 6. Solvent screening (s) averaged over all configurations as a function of the distance between the monomers. Top panel: B3LYP; bottom panel: CCSD.

irregular, and they do not yet converge to a single value even at the longest distance. The CCSD results, on the other hand, start rather differently with the $L_a–L_a$ and $L_a–L_b$ screening clustered together as well as the $L_b–L_b$ and $L_b–L_a$ screening. However, the CCSD results soon converge to a similar value that reaches a plateau around 0.66−0.67, which is in good agreement with the Onsager result. Such agreement is reasonable because indole is a small chromophore, and the PCM solvation resembles that obtained with the Onsager model at larger distances.

The screening computed for the stacked configuration is shown in Figure 7, where the top plot is still for B3LYP and the
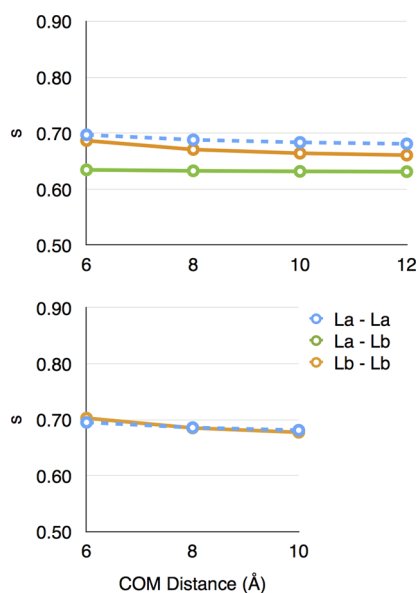
Figure 7. Solvent screening (s) for the stacked configuration as a function of the distance between the monomers. Top panel: B3LYP; bottom panel: CCSD.

bottom for CCSD. In both cases, the screening for the $L_b–L_a$ case is not reliable because the values of the coupling for the transfer are rather small. The same is true for the $L_a–L_b$ coupling with CCSD. For the $L_a–L_a$ and $L_b–L_b$ couplings, the trends are similar to the average case: a slightly larger screening is found at smaller distances, which reaches a plateau at longer distances. For B3LYP, the screening does not converge to the same value. The screening computed with CCSD, on the other hand, converges to a value of 0.68 very quickly.

The screening for the T-shaped configuration is reported in Figure 8. In this case, the curve for the $L_b–L_a$ coupling is not reported because it is completely unreliable due to very small values of the coupling that make the formula for the solvent screening numerically unstable. For all the other cases, the trends are very similar to what was found previously. The B3LYP data (top panel in the figure) are more scattered even at larger distances (s varies from 0.68 to 0.71). Conversely, the screening computed with CCSD converges rapidly to a value of 0.69−0.70 for all the energy transfers.

5. DISCUSSION AND CONCLUSIONS

In this work, we present the implementation and the first calculations of electronic couplings at CCSD level of theory in gas phase and in solution. We apply this method to an important model system: the dimer of indole. Indole represents
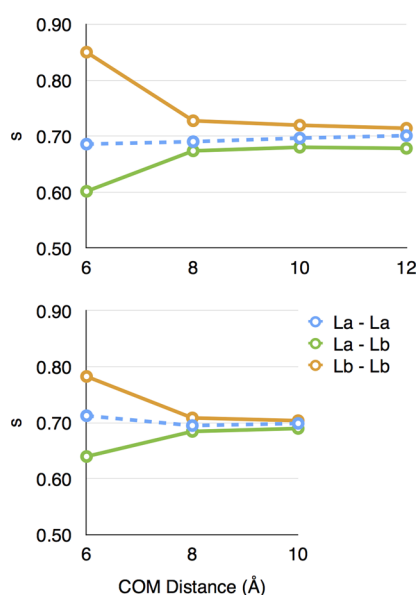
Figure 8. Solvent screening (s) for the T-shaped configuration as a function of the distance between the monomers. Top panel: B3LYP; bottom panel: CCSD.

the main chromophoric moiety of tryptophan, an amino acid widely used as a fluorescence probe in RET studies and responsible for the intrinsic fluorescence of proteins, which often involves transfers among tryptophans prior to emission. We compare this high level of theory with an approximate density functional, B3LYP, which is still one of the most popular methods in quantum chemical calculations. We include rather short distances between the chromophores in our test set to maximize the coupling and explore the differences between the levels of theory. We report results obtained from averaging of multiple relative orientations between the chromophores at various distances. We also isolate two specific configurations shown in Figure 1, stacked and T-shaped, to examine trends without the bias of an incomplete sampling in the averaged data set.

We consider the two excited states, L_a and L_b, mainly responsible for the fluorescent properties of tryptophan, for a total of four possible couplings. Our calculations show that B3LYP underestimates the coupling between the L_a state of the indole molecules, which is the charge transfer state, compared to CCSD. The underestimation is consistent with the smaller magnitude of the electric transition dipole, shown as dipole strength in Table 1. In turn, the smaller value of dipole and oscillator strength compared to CCSD is consistent with the overdelocalization of the electronic density typical of global GGA functionals, which reduces the charge transfer character of this state. Conversely, B3LYP overestimates the L_b–L_b coupling compared to CCSD, again consistent with the relative magnitude of the dipole strength. However, the overestimation is larger than one would have expected by consideration of the dipole strength magnitude alone. Interestingly, the ratio between B3LYP and CCSD results for the average values of V^2 in the L_a–L_a and L_b–L_b cases is 2 and 0.5, respectively. The difference between the two levels of theory for the cross couplings varies between the average case and the two selected configurations with B3LYP either under or overestimating the CCSD results.

The decay rate is usually close to the sixth power law of Förster theory, although it is slower in cases like L_a–L_a and L_a–L_b after averaging over the various configurations, where it is between the fourth and fifth power. The other different case is for the T-shaped configuration, where the distances considered put the two systems close enough to show a considerable deviation from the Förster model with values for the fitting on the order of 3.6–5.1. The difference between the methods is not large, except for some cases like L_b–L_a, where there is an order of magnitude difference. In general, CCSD predicts slightly faster decays than B3LYP.

The role of solvation is consistent across levels of theory. The solvent tends to reduce the value of the coupling for the configuration average and for the stacked configuration, whereas it shows the opposite behavior for the T-shaped configuration. The solvent effect is considerably smaller for the averaged results than for the individual configurations, indicating that the shift is in opposite directions for the various configurations such that it compensates during the averaging. The analysis of the solvent screening allows for separation of the direct effect of the solvent from the effect of the polarization of the wave function. The results, shown in Figures 6–8, indicate a smooth convergence of the CCSD results with the distance toward a value that is very close to that predicted by the Onsager model. This limit value for the solvent screening is reasonable because the PCM cavity of such small molecules can be approximated as a sphere at large distances, exactly as done in the Onsager model. The B3LYP results, conversely, show a much less smooth convergence.

Although approximate QM methods are often the only choice when large molecular or supramolecular systems are considered, it is important to know how reliable they are for a meaningful comparison with experiments. The method presented in this work provides a useful tool for benchmarking approximate levels of theory in the evaluation of the electronic coupling between a donor and an acceptor chromophore. This is important, for instance, for states with partial charge-transfer character where the effect of the environment is large and TD-DFT methods have difficulties. Indeed, a correct assignment of the relative position of L_a and L_b states is important to identify the emitting state in tryptophan.[60] Future development will involve extending the present methodology to the mixed polarizable QM/MM methodology we have recently presented to study energy transfer phenomena in heterogeneous biological environments.[19]

■ ASSOCIATED CONTENT

Ⓢ Supporting Information

The Supporting Information is available free of charge on the ACS Publications website at DOI: 10.1021/acs.jctc.5b00720.

> The averaged values of V^2 in $(cm^{-1})^2$ are reported in Supporting Tables 1–4 for B3LYP and CCSD in gas phase and in solution, and the corresponding standard deviations are reported in Supporting Tables 5–8; the structures of the dimers for the different configurations used for the calculations (for the 8 Å distance) are reported in Supporting Tables 9–38 (PDF)

■ AUTHOR INFORMATION

Corresponding Author

*E-mail: mcaricato@ku.edu.

■ REFERENCES

(1) Blankenship, R. *Molecular Mechanisms of Photosynthesis*, 2nd ed.; Wiley-Blackwell, 2014.

(2) Andrews, D. L.; Curutchet, C.; Scholes, G. D. Resonance Energy Transfer: Beyond the Limits. *Laser Photonics Rev.* **2011**, *5*, 114−123.

(3) Scholes, G. D.; Fleming, G. R.; Olaya-Castro, A.; Van Grondelle, R. Lessons from Nature about Solar Light Harvesting. *Nat. Chem.* **2011**, *3*, 763−774.

(4) Fleming, G. R.; Schlau-Cohen, G. S.; Amarnath, K.; Zaks, J. Design Principles of Photosynthetic Light-Harvesting. *Faraday Discuss.* **2012**, *155*, 27−41.

(5) Frischmann, P. D.; Mahata, K.; Würthner, F. Powering the Future of Molecular Artificial Photosynthesis with Light-Harvesting Metallosupramolecular Dye Assemblies. *Chem. Soc. Rev.* **2013**, *42*, 1847.

(6) Saikin, S. K.; Eisfeld, A.; Valleau, S.; Aspuru-Guzik, A. Photonics Meets Excitonics: Natural and Artificial Molecular Aggregates. *Nanophotonics* **2013**, *2*, 21−38.

(7) Förster, T. Energiewanderung und Fluoreszenz. *Naturwissenschaften* **1946**, *33*, 166−175.

(8) Förster, T. Zwischenmolekulare Energiewanderung und Fluoreszenz. *Ann. Phys.* **1948**, *2*, 55−75.

(9) Hsu, C. P.; Fleming, G. R.; Head-Gordon, M. Excitation Energy Transfer in Condensed Media. *J. Chem. Phys.* **2001**, *114*, 3065−3072.

(10) Scholes, G. D. Long-Range Resonance Energy Transfer in Molecular Systems. *Annu. Rev. Phys. Chem.* **2003**, *54*, 57−87.

(11) Iozzi, M. F.; Mennucci, B.; Tomasi, J.; Cammi, R. Excitation Energy Transfer (EET) between Molecules in Condensed Matter: A Novel Application of the Polarizable Continuum Model (PCM). *J. Chem. Phys.* **2004**, *120*, 7029.

(12) Curutchet, C.; Mennucci, B. Toward a Molecular Scale Interpretation of Excitation Energy Transfer in Solvated Bichromophoric Systems. *J. Am. Chem. Soc.* **2005**, *127*, 16733−16744.

(13) Hsu, C. P.; You, Z. Q.; Chen, H. C. Characterization of the Short-Range Couplings in Excitation Energy Transfer. *J. Phys. Chem. C* **2008**, *112*, 1204−1212.

(14) Chen, H.-C.; You, Z.-Q.; Hsu, C.-P. The Mediated Excitation Energy Transfer: Effects of Bridge Polarizability. *J. Chem. Phys.* **2008**, *129*, 084708.

(15) Hsu, C.-P. The Electronic Couplings in Electron Transfer and Excitation Energy Transfer. *Acc. Chem. Res.* **2009**, *42*, 509−518.

(16) Muñoz Losa, A.; Curutchet, C.; Krueger, B. P.; Hartsell, L. R.; Mennucci, B. Fretting about FRET: Failure of the Ideal Dipole Approximation. *Biophys. J.* **2009**, *96*, 4779−4788.

(17) Beljonne, D.; Curutchet, C.; Scholes, G. D.; Silbey, R. J. Beyond Förster Resonance Energy Transfer in Biological and Nanoscale Systems. *J. Phys. Chem. B* **2009**, *113*, 6583−6599.

(18) Subotnik, J. E.; Vura-Weis, J.; Sodt, A. J.; Ratner, M. A. Predicting Accurate Electronic Excitation Transfer Rates via Marcus Theory with Boys or Edmiston-Ruedenberg Localized Diabatization. *J. Phys. Chem. A* **2010**, *114*, 8665−8675.

(19) Curutchet, C.; Kongsted, J.; Muñoz Losa, A.; Hossein-Nejad, H.; Scholes, G. D.; Mennucci, B. Photosynthetic Light-Harvesting Is Tuned by the Heterogeneous Polarizable Environment of the Protein. *J. Am. Chem. Soc.* **2011**, *133*, 3078−3084.

(20) Mennucci, B.; Curutchet, C. The Role of the Environment in Electronic Energy Transfer: a Molecular Modeling Perspective. *Phys. Chem. Chem. Phys.* **2011**, *13*, 11538−11550.

(21) Scholes, G. D.; Curutchet, C.; Mennucci, B.; Cammi, R.; Tomasi, J. How Solvent Controls Electronic Energy Transfer and Light Harvesting. *J. Phys. Chem. B* **2007**, *111*, 6978−6982.

(22) Ridley, J.; Zerner, M. Intermediate Neglect of Differential Overlap Technique for Spectroscopy - Pyrrole and Azines. *Theor. Chim. Acta* **1973**, *32*, 111−134.

(23) Bartlett, R.; Musiał, M. Coupled-Cluster Theory in Quantum Chemistry. *Rev. Mod. Phys.* **2007**, *79*, 291−352.

(24) Sekino, H.; Bartlett, R. A Linear Response, Coupled-Cluster Theory for Excitation-Energy. *Int. J. Quantum Chem.* **1984**, *26*, 255−265.

(25) Koch, H.; Jorgensen, P. Coupled Cluster Response Functions. *J. Chem. Phys.* **1990**, *93*, 3333−3344.

(26) Stanton, J. F.; Bartlett, R. The Equation of Motion Coupled-Cluster Method - A Systematic Biorthogonal Approach to Molecular-Excitation Energies, Transition-Probabilities, and Excited-State Properties. *J. Chem. Phys.* **1993**, *98*, 7029−7039.

(27) Cammi, R. Quantum Cluster Theory for the Polarizable Continuum Model. I. The CCSD Level with Analytical First and Second Derivatives. *J. Chem. Phys.* **2009**, *131*, 164104.

(28) Caricato, M.; Scalmani, G.; Trucks, G. W.; Frisch, M. J. Coupled Cluster Calculations in Solution with the Polarizable Continuum Model of Solvation. *J. Phys. Chem. Lett.* **2010**, *1*, 2369−2373.

(29) Cammi, R. Coupled-Cluster Theories for the Polarizable Continuum Model. II. Analytical Gradients for Excited States of Molecular Solutes by the Equation of Motion Coupled-Cluster Method. *Int. J. Quantum Chem.* **2010**, *110*, 3040−3052.

(30) Caricato, M. Absorption and Emission Spectra of Solvated Molecules with the EOM−CCSD−PCM Method. *J. Chem. Theory Comput.* **2012**, *8*, 4494−4502.

(31) Caricato, M. Exploring Potential Energy Surfaces of Electronic Excited States in Solution with the EOM-CCSD-PCM Method. *J. Chem. Theory Comput.* **2012**, *8*, 5081−5091.

(32) Cammi, R. Coupled-Cluster Theory for the Polarizable Continuum Model. III. A Response Theory for Molecules in Solution. *Int. J. Quantum Chem.* **2012**, *112*, 2547−2560.

(33) Caricato, M. Implementation of the CCSD-PCM Linear Response Function for Frequency Dependent Properties in Solution: Application to Polarizability and Specific Rotation. *J. Chem. Phys.* **2013**, *139*, 114103.

(34) Caricato, M. A Comparison between State-Specific and Linear-Response Formalisms for the Calculation of Vertical Electronic Transition Energy in Solution with the CCSD-PCM Method. *J. Chem. Phys.* **2013**, *139*, 044116.

(35) Lee, C.; Yang, W.; Parr, R. G. Development of the Colle-Salvetti Correlation-Energy Formula into a Functional of the Electron Density. *Phys. Rev. B: Condens. Matter Mater. Phys.* **1988**, *37*, 785−789.

(36) Becke, A. D. Density-Functional Thermochemistry 0.3. The Role of Exact Exchange. *J. Chem. Phys.* **1993**, *98*, 5648−5652.

(37) Stephens, M. D.; Saven, J. G.; Skinner, J. L. Molecular Theory of Electronic Spectroscopy in Nonpolar Fluids: Ultrafast Solvation Dynamics and Absorption and Emission Line Shapes. *J. Chem. Phys.* **1997**, *106*, 2129.

(38) Nolting, D.; Marian, C.; Weinkauf, R. Protonation Effect on the Electronic Spectrum of Tryptophan in the Gas Phase. *Phys. Chem. Chem. Phys.* **2004**, *6*, 2633.

(39) Grégoire, G.; Jouvet, C.; Dedonder, C.; Sobolewski, A. L. Ab initio Study of the Excited-State Deactivation Pathways of Protonated Tryptophan and Tyrosine. *J. Am. Chem. Soc.* **2007**, *129*, 6223−6231.

(40) Callis, P. R. Predicting Fluorescence Lifetimes and Spectra of Biopolymers. *Methods Enzymol.* **2011**, *487*, 1−38.

(41) Knox, R. S.; van Amerongen, H. Refractive Index Dependence of the Förster Resonance Excitation Transfer Rate. *J. Phys. Chem. B* **2002**, *106*, 5289−5293.

(42) Fückel, B.; Köhn, A.; Harding, M. E.; Diezemann, G.; Hinze, G.; Basché, T.; Gauss, J. Theoretical Investigation of Electronic Excitation Energy Transfer in Bichromophoric Assemblies. *J. Chem. Phys.* **2008**, *128*, 074505.

(43) Christiansen, O.; Jorgensen, P.; Hattig, C. Response functions from Fourier component variational perturbation theory applied to a time-averaged quasienergy. *Int. J. Quantum Chem.* **1998**, *68*, 1−52.

(44) Koch, H.; Kobayashi, R.; Demeras, A.; Jorgensen, P. Calculation of Size-Intensive Transition Moments from the Coupled Cluster Singles and Doubles Linear-Response Function. *J. Chem. Phys.* **1994**, *100*, 4393−4400.

(45) Caricato, M.; Trucks, G. W.; Frisch, M. J. On the Difference between the Transition Properties Calculated with Linear Response- and Equation of Motion-CCSD Approaches. *J. Chem. Phys.* **2009**, *131*, 174104.

(46) Dunning, T. H., Jr Gaussian Basis Sets for Use in Correlated Molecular Calculations. I. The Atoms Boron through Neon and Hydrogen. *J. Chem. Phys.* **1989**, *90*, 1007−1023.

(47) Kendall, R. A.; Dunning, T. H., Jr; Harrison, R. J. Electron Affinities of the First-Row Atoms Revisited. Systematic Basis Sets and Wave Functions. *J. Chem. Phys.* **1992**, *96*, 6796−6806.

(48) Lipparini, F.; Scalmani, G.; Mennucci, B.; Cances, E.; Caricato, M.; Frisch, M. J. A Variational Formulation of the Polarizable Continuum Model. *J. Chem. Phys.* **2010**, *133*, 014106.

(49) Marenich, A. V.; Cramer, C. J.; Truhlar, D. G. Universal Solvation Model Based on Solute Electron Density and on a Continuum Model of the Solvent Defined by the Bulk Dielectric Constant and Atomic Surface Tensions. *J. Phys. Chem. B* **2009**, *113*, 6378−6396.

(50) Pascual-ahuir, J. L.; Silla, E.; Tuñon, I. GEPOL: An Improved Description of Molecular Surfaces. III. A New Algorithm for the Computation of a Solvent-Excluding Surface. *J. Comput. Chem.* **1994**, *15*, 1127−1138.

(51) Scalmani, G.; Frisch, M. J. Continuous Surface Charge Polarizable Continuum Models of Solvation. I. General Formalism. *J. Chem. Phys.* **2010**, *132*, 114110.

(52) Frisch, M. J.; Trucks, G. W.; Schlegel, H. B.; Scuseria, G. E.; Robb, M. A.; Cheeseman, J. R.; Scalmani, G.; Barone, V.; Mennucci, B.; Petersson, G. A.; Nakatsuji, H.; Caricato, M.; Li, X.; Hratchian, H. P.; Izmaylov, A. F.; Bloino, J.; Zheng, G.; Sonnenberg, J. L.; Hada, M.; Ehara, M.; Toyota, K.; Fukuda, R.; Hasegawa, J.; Ishida, M.; Nakajima, T.; Honda, Y.; Kitao, O.; Nakai, H.; Vreven, T.; Montgomery, J. A., Jr.; Peralta, J. E.; Ogliaro, F.; Bearpark, M.; Heyd, J. J.; Brothers, E.; Kudin, K. N.; Staroverov, V. N.; Keith, T.; Kobayashi, R.; Normand, J.; Raghavachari, K.; Rendell, A.; Burant, J. C.; Iyengar, S. S.; Tomasi, J.; Cossi, M.; Rega, N.; Millam, J. M.; Klene, M.; Knox, J. E.; Cross, J. B.; Bakken, V.; Adamo, C.; Jaramillo, J.; Gomperts, R.; Stratmann, R. E.; Yazyev, O.; Austin, A. J.; Cammi, R.; Pomelli, C.; Ochterski, J. W.; Martin, R. L.; Morokuma, K.; Zakrzewski, V. G.; Voth, G. A.; Salvador, P.; Dannenberg, J. J.; Dapprich, S.; Parandekar, P. V.; Mayhall, N. J.; Daniels, A. D.; Farkas, O.; Foresman, J. B.; Ortiz, J. V.; Cioslowski, J.; Fox, D. J. *Gaussian Development Version*, revision h.09+ ed.; Gaussian, Inc.: Wallingford, CT, 2010.

(53) Strickland, E. H.; Billups, C. Oscillator strengthes of the 1La and 1Lb absorption bands of tryptophan and several other indoles. *Biopolymers* **1973**, *12*, 1989−1995.

(54) Lami, H. Presence of a low-lying "Rydberg" band in the vapour phase absorption spectra of indole and 1-methyl indole. *Chem. Phys. Lett.* **1977**, *48*, 447−450.

(55) Meng, X.; Harricharran, T.; Juszczak, L. J. A Spectroscopic Survey of Substituted Indoles Reveals Consequences of a Stabilized 1Lb Transition. *Photochem. Photobiol.* **2013**, *89*, 40−50.

(56) Brisker-Klaiman, D.; Dreuw, A. Explaining Level Inversion of the L aand L bStates of Indole and Indole Derivatives in Polar Solvents. *ChemPhysChem* **2015**, *16*, 1695−1702.

(57) Sobolewski, A.; Domcke, W.; Dedonder-Lardeux, C.; Jouvet, C. Excited-State Hydrogen Detachment and Hydrogen Transfer Driven by Repulsive $^1\pi\sigma^*$ States: A New Paradigm for Nonradiative Decay in Aromatic Biomolecules. *Phys. Chem. Chem. Phys.* **2002**, *4*, 1093−1100.

(58) Curutchet, C.; Muñoz Losa, A.; Monti, S.; Kongsted, J.; Scholes, G. D.; Mennucci, B. Electronic Energy Transfer in Condensed Phase Studied by a Polarizable QM/MM Model. *J. Chem. Theory Comput.* **2009**, *5*, 1838−1848.

(59) Neugebauer, J.; Curutchet, C.; Muñoz Losa, A.; Mennucci, B. A Subsystem TDDFT Approach for Solvent Screening Effects on Excitation Energy Transfer Couplings. *J. Chem. Theory Comput.* **2010**, *6*, 1843−1851.

(60) Callis, P. R. Binding Phenomena and Fluorescence Quenching. II: Photophysics of Aromatic Residues and Dependence of Fluorescence Spectra on Protein Conformation. *J. Mol. Struct.* **2014**, *1077*, 22−29.